

# Solvothermal synthesis derived Co-Ga codoped ZnO diluted magnetic degenerated semiconductor nanocrystals

a, b, \*

a

a, c

a, d

a

Andris Sutka <sup>a, b, \*</sup>, Tanel Kaambre <sup>a</sup>, Urmas Joost <sup>a</sup>, Kuno Kooser <sup>a</sup>, Mati Kook <sup>a</sup>, Roberto Felix Duarte <sup>e</sup>, Vambola Kisand <sup>a</sup>, Mikhael Maiorov <sup>f</sup>, Nicola Dobelin <sup>g</sup>, Krisjanis Smits <sup>h</sup>

<sup>a</sup> Institute of Physics, University of Tartu, W. Ostwaldi Street 1, 50411, Tartu, Estonia

<sup>b</sup> Research Laboratory of Functional Materials Technologies, Faculty of Materials Science and Applied Chemistry, Riga Technical University, Paula Valdena 3/7, 1048, Riga, Latvia

<sup>c</sup> Surface Science Group, Photonics Laboratory, Tampere University of Technology, PO BOX 692, FI-33101, Tampere, Finland

<sup>d</sup> Department of Physics and Astronomy, University of Turku, FIN-20014, Turku, Finland

<sup>e</sup> Helmholtz Centre Berlin for Materials and Energy, 14109, Berlin, Germany

<sup>f</sup> Institute of Physics, University of Latvia, Miera 32, 2169, Salaspils, Latvia

<sup>g</sup> RMS Foundation, Bischmattstrasse 12, 2544, Bettlach, Switzerland

<sup>h</sup> Institute of Solid State Physics, University of Latvia, Kangaraga 8, 1063, Riga, Latvia

## article info

### Keywords:

ZnO

Plasmonic nanocrystals

Doping

Diluted magnetic semiconductors

Degenerated semiconductors

Solvothermal synthesis

## abstract

Here we are reporting solvothermal synthesis derived diluted magnetic and plasmonic Co-Ga co-doped ZnO nanocrystals with high magnetization values (from 1.02 to 4.88 emu/g) at room temperature. Co-Ga co-doped ZnO nanocrystals show up to 2 fold increase in saturation magnetization compared to Co doped ZnO nanocrystals at the same Co concentration, with the observed room temperature magnetization higher than previously reported values for multifunctional magnetic and plasmonic nanocrystals, and the effect of Ga suggesting some role of the correspondingly introduced itinerant charge. While at the lowest Ga content the nanoparticles appear homogeneously doped, we note that already a moderate Ga content of several percent triggers a fraction of Co to segregate in metallic form in the bulk of the nanoparticles. However, the amount of segregated Co is not sufficient to account for the total effect, whereas a dominating contribution to the observed magnetism has to be related to itinerant charge mediated exchange interactions.

## 1. Introduction

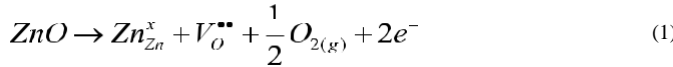
A variety of aliovalent donor dopants such as Al [1e3], Ga [3e5], Ge [6] and In Refs. [3,7] have been used to produce ZnO based plasmonic nanocrystals. When effectively doped, ZnO becomes a degenerate semiconductor with high concentration of delocalized conduction band electrons and exhibits surface plasmon resonance absorption features in the infrared spectral range [8]. Plasmonic ZnO nanocrystals potentially can be used for various applications e in medicine for IR absorption driven heat treatment of tissue [9], electrochromics [10e13], visible light transparent elastomeric

piezoresistive composite materials [14], transparent conductive electrodes [15], IR-absorbing coatings [3,16], dynamically modifiable photonic devices [17] and biosensors [18]. From the aspect of plasmonics, more efficient doping e in terms of obtaining a higher density of delocalized electrons in the semiconductor lattice e occurs in synthesis environments that shifts the equilibrium between oxygen adsorption and desorption towards the desorption, which can be achieved under reducing conditions. Degenerated semiconductor plasmonic metal oxide nanocrystals have been previously synthesized by colloidal heat up method [5], thermal decomposition of cation precursors in a mixture of hot solvent (octadecene) and capping agents (viz. oleic acid, oleylamine) [19], cationic precursor hot injection into a solution of reducing agent [1], as well as ethanol solvothermal synthesis [14]. In solvothermal synthesis organic solvents (such as ethanol, butanol) act as reducing agents and are therefore prone to create electronic point

\* Corresponding author. Institute of Physics, University of Tartu, W. Ostwaldi Street 1, 50411, Tartu, Estonia.

E-mail address: andris.sutka@rtu.lv (A. Sutka).

defects in ZnO [20]. The reaction mechanism for oxygen vacancy and electron formation under reducing conditions in ZnO can be written (in Kroger-Vink notation) as:



where  $V_O$  is oxygen vacancy with effective charge  $\pm 2$ ,  $Zn_{Zn}^x$  is a Zn at a Zn lattice site (effective charge zero),  $O_{2(g)}$  is molecular oxygen (gas) released from lattice,  $e$  is free electron.

Transition metal (TM) doped ZnO is also one of the most studied diluted magnetic semiconductor oxides (DMSO). ZnO doped with Co [20e23], Fe [24], Ni [25] and Mn [20,26e28] exhibit room temperature ferromagnetism when interaction between delocalized charge carriers (electrons or holes) and localized d spins occurs [21,22].

The absence of ferromagnetism has been observed in TM doped ZnO free from point defects [21]. Point defects, such as aliovalent donor or acceptor dopants, oxygen vacancies or zinc interstitials in ZnO crystal lattice can be compensated by introduction of appropriate numbers of electrons or holes which have been recognized to have a crucial role in mediating the magnetic coupling [29,30]. Experimental evidence of such unexpectedly prominent role of itinerant electrons in mediating magnetic interactions in some doped oxides has been in a few recent years been put forward for Mn-Sn codoped  $In_2O_3$  (Mn-ITO) [31,32] and Fe-Sn codoped  $In_2O_3$  (Fe-ITO) [33e36] diluted magnetic degenerated semiconductor oxides (DMDSO). These materials have potential for spintronic applications with ongoing research into approaches to manipulate magnetic exchange coupling strength [31].

In the present work a straightforward and readily industrializable ethanol solvothermal synthesis is used to obtain DMDSO in the form of Co-Ga codoped ZnO (Co-GZO) nanoparticles. Recently we already demonstrated ethanol solvothermal synthesis as a straightforward route to obtain plasmonic Al doped ZnO nano-crystals [14], which allows us to predict that solvothermal method could be quite suitable for obtaining DMDSO. Indeed, the synthe-sized Co-GZO nanocrystals in this study exhibit stronger delocalized electron mediated magnetic coupling than what has previously been observed for TM-ITO nanocrystals [29e33]. A possible drawback of solvothermal method is relatively large shape and size distribution of obtained nanocrystals, yielding wide plasmonic absorption peaks [14], but at the same time the synthesis without ligands allows avoiding electrically insulating barriers between nanocrystals in the solid state, which is important for practical applications [37,38]. Herein we also study TM dopant clustering and its effect on magnetic properties. There is always a question whether the origin of room temperature ferromagnetism in DMDSO is magnetic interaction between localized d spins of magnetic dopants and delocalized electrons or metallic clusters of segregated TM dopant [39e41]. In the present work we demonstrate that aliovalent donor dopants have significant influence on Co cluster formation, and that metal clusters and (quasi-)uniform inclusions of the TM dopant in the crystal lattice co-exist in Co-Ga codoped ZnO DMDSO.

## 2. Experimental section

The nanocrystals used for this study were synthesized by ethanol solvothermal method as described in our previous works [14,42,43]. Zinc acetate dihydrate ( $Zn(CH_3COO)_2 \cdot 2H_2O$ ), cobalt acetate tetrahydrate ( $(CH_3COO)_2Co \cdot 4H_2O$ ) and Ga chloride ( $GaCl_3$ ) in required molar ratio were dissolved in absolute ethanol at total concentration 0.1 M at 80 C. Next, 1 M NaOH solution in absolute ethanol was added to salt solution at volumetric ratio 2:1 and

stirred for next 3 h. Then solution was filled in Teflon sealed stainless steel autoclave 90% by volume, tightly closed and left for solvothermal treatment at 150 C for 24 h. Obtained nanocrystals were washed in absolute ethanol by centrifugation.

X-ray diffraction (XRD) analysis: XRD patterns were measured by UltimapX-ray diffractometer (Rigaku, Japan) using Cu-K $\alpha$  radiation. Electron microscopy at high magnification was performed using high resolution scanning electron microscopy (SEM, Helios Nanolab, FEI) and transmission electron microscopy (TEM, Tecnai G2 F20, FEI) operated at 200 kV. The hard X-ray photoelectron spectroscopy (HAXPES) measurements (with an overall resolution of 0.4 eV) were done on the HIKE experimental station at the KMC-1 beamline at the BESSY-II synchrotron source (Helmholtz-Zentrum Berlin, Germany) [44]. Transmittance and light absorbance of nanopowder samples was measured by Shimadzu UV-vis spec-trophotometer, UV-3700 (Shimadzu Scientific Instruments Kyoto, Japan). Particles for transmittance measurements were dispersed at a concentration of 0.1 mg/ml in tetrachloroethylene and stabilized by adding a mixture of oleylamine and dodecylbenzenesulfonic acid (0.01 mg/ml) in ratio 1:1. For light absorption measurements barium sulphate coated integrating sphere ISR-240A was used.

The luminescence measurements were carried out at low temperature using closed cycle helium cryostat. For luminescence excitation YAG laser FQSS266 (CryLas GmbH) 4th harmonic at 266 nm (4.66 eV) was used. The luminescence spectra were recorded using an Andor Shamrock B-303i spectrograph equipped with a CCD camera (Andor DU-401A-BV). For luminescence measurements, the same amount of all powder samples was lightly pressed into small uniformly sized stainless steel cells. This enabled a quantitative comparison of the luminescence intensities. The spectral correction was applied.

Magnetic properties were measured for sample powders filled in special plastic capsule using a vibrating sample magnetometer (Lake Shore Cryotronic Co., Model 7404 VSM, USA) at room temperature for fields up to 10 kOe. The sample holder was measured separately and its signal was subtracted from the full raw magnetization signal of each sample in the holder capsule.

## 3. Results and discussion

X-ray diffractograms for synthesized ZnO, Co-ZnO, GZO and Co-GZO nanocrystals are demonstrated in Fig. 1, where pristine ZnO, Ga doped ZnO and Co doped ZnO exhibit wurtzite structure (ICDD 01-080-4433) and no adjacent phases are observed even for the compositions with the large amount of single element dopant, i.e.,  $Zn_{0.85}Ga_{0.15}O$  and  $Zn_{0.90}Co_{0.10}O$ . Fig. 1 shows that when increasing the doping level, an initial increase in both the a-axis and the c-axis lattice constants is seen to continue up to the TM dopant content of approximately 5e7% (cationic), after which this growth not only stops, but is even reversed (a plausible cause of the latter being increased TM dopant segregation at higher doping values). The increase in lattice constant in Co doped wurtzite ZnO is an indicator of an effective Zn substitution by Co [45]. All the presented compositions have higher lattice constants than pristine ZnO. When co-dopant Ga gradually substitutes Zn in  $Zn_{0.95}Co_{0.05}O$  and total dopant concentration exceeds 10% of Zn, peaks related to Co nanoscale metal clusters appear (Fig. 1). Similar Co metal (ICDD 01-089-7373) clustering is observed for the other codoped  $Zn_{0.9-x}Ga_{0.1}Co_xO$  samples where x is varied from 0.025 to 0.10.

As reported by B. Cheng and E.T. Samulski [46] and observed here, ethanol solvothermal synthesis of ZnO yields nanowires (SEM images are demonstrated in Fig. 2); the obtained pristine ZnO nanowire average diameter is around 50 nm and length up to 1  $\mu$ m, and the morphology is not noticeably changed under Co doping. However, adding Ga obviously changes the morphology, reducing

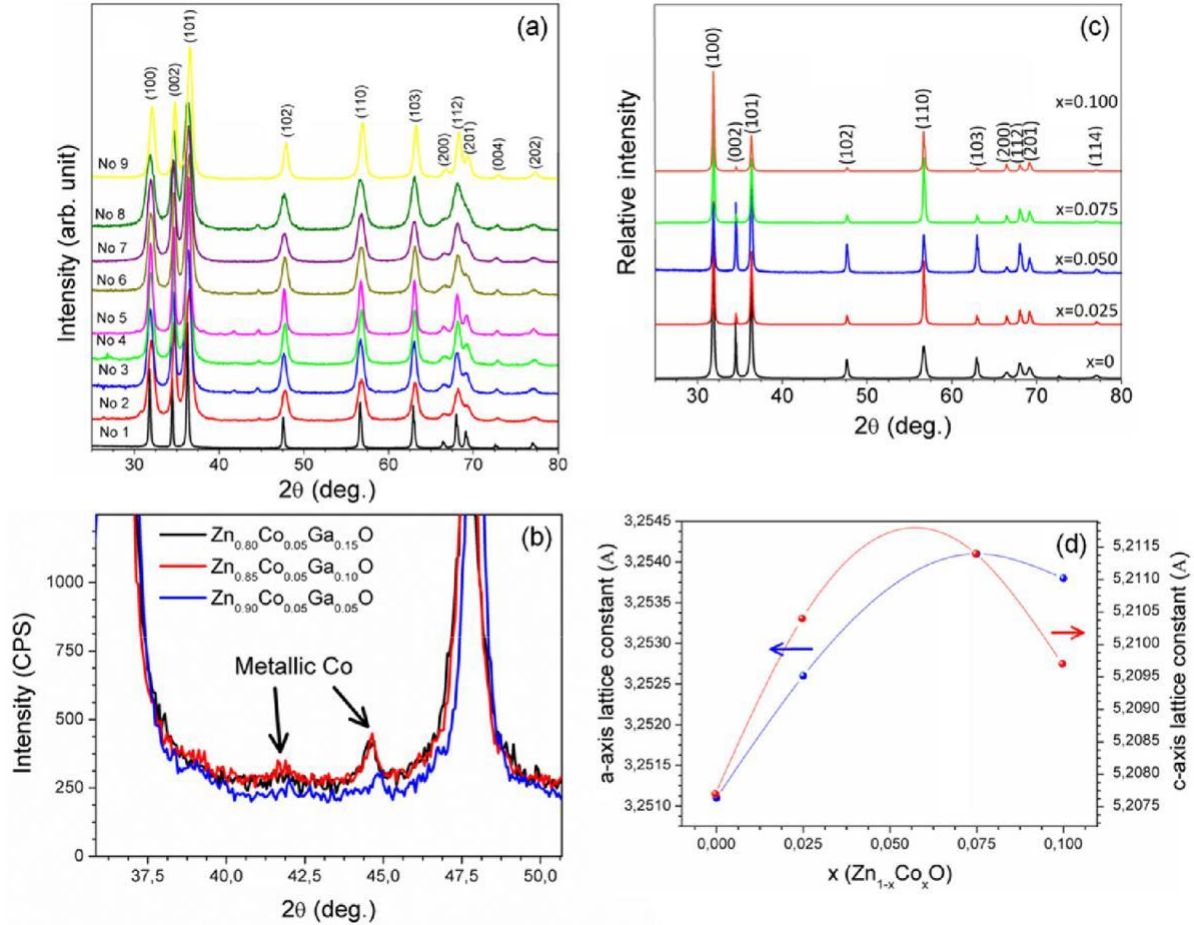


Fig. 1. (a) X-ray diffractograms for various samples - No 1: ZnO, No 2: Zn<sub>0.875</sub>Ga<sub>0.10</sub>Co<sub>0.025</sub>O, No 3: Zn<sub>0.85</sub>Ga<sub>0.10</sub>Co<sub>0.05</sub>O, No 4: Zn<sub>0.825</sub>Ga<sub>0.10</sub>Co<sub>0.075</sub>O, No 5: Zn<sub>0.80</sub>Ga<sub>0.10</sub>Co<sub>0.10</sub>O, No 6: Zn<sub>0.81</sub>Ga<sub>0.14</sub>Co<sub>0.05</sub>O, No 7: Zn<sub>0.90</sub>Ga<sub>0.10</sub>O, No 8: Zn<sub>0.80</sub>Ga<sub>0.15</sub>Co<sub>0.05</sub>O, No 9: Zn<sub>0.90</sub>Ga<sub>0.05</sub>Co<sub>0.05</sub>O. (b) XRD patterns of 5% (at.) Co, but varied Ga content samples in the angular range of metallic Co peaks, (c) the X-ray diffractograms of Zn<sub>1-x</sub>CoxO over a wide compositional range (not indicating any Co clustering) and (d) the dependence of Zn<sub>1-x</sub>CoxO lattice constants on Co content x.

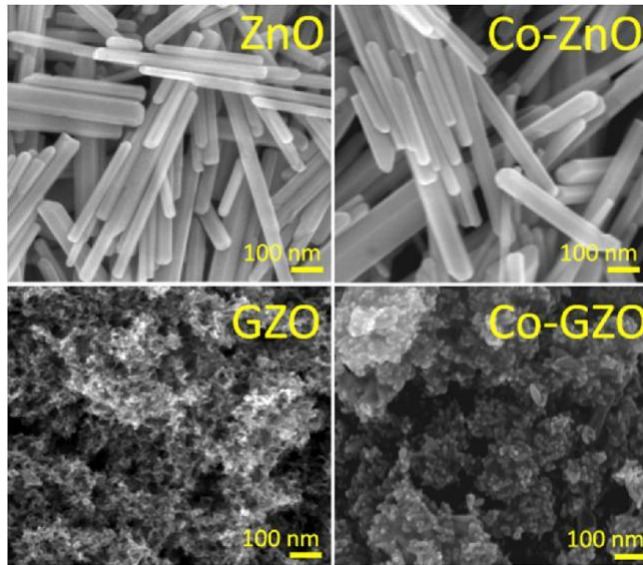
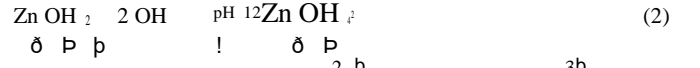


Fig. 2. Typical SEM images of ZnO, Zn<sub>0.9</sub>Co<sub>0.10</sub>O, Zn<sub>0.9</sub>Ga<sub>0.10</sub>O and Co-Ga co-doped ZnO Zn<sub>0.85</sub>Ga<sub>0.05</sub>Co<sub>0.10</sub>O nanocrystals.

the size (to below 10 nm) and the aspect ratio (1e5) of the synthesis product. TEM image of Zn<sub>0.9</sub>Ga<sub>0.10</sub>O nanocrystals is demonstrated in Fig. 3. The hypervalent donor doping increases (delocalized) charge density, but under alkaline conditions the ZnO crystal growth occurs from zincate ion ( $Zn(OH)_4^{2-}$ ) units [47], which form at pH values above 12 according to:



Free electrons introduced by  $Zn^{2+}$  substitution with  $Ga^{3+}$  make it difficult for the zincate ions to diffuse to the crystal surface because of Coulomb repulsion [47].

Fig. 4 presents Kubelka-Munk absorption spectra of ZnO, Co doped ZnO, Ga doped Co and Co-Ga co-doped ZnO powders. The spectrum of the non-doped nanoparticles is defined by the band gap of ZnO, with a steep rise in absorptivity at around 375 nm (3.3 eV) [48]. The Co doped ZnO samples (Fig. 4 (a)) exhibit additional bands at longer wavelengths (in the visible and infrared range), well separated from the fundamental absorption edge. The well separated partially resolved peaks centered at around 568, 611 and 654 nm, as well as at 1325, 1422 and 1645 nm are related to electronic d-d transitions between crystal field split levels of  $Co^{2+}$  ion with  $3d^7$  high spin electron configuration in tetrahedral coordination of  $O^{2-}$  ions [21,49]. The observed spectral features and the intensity increase of this absorption band with increased Co

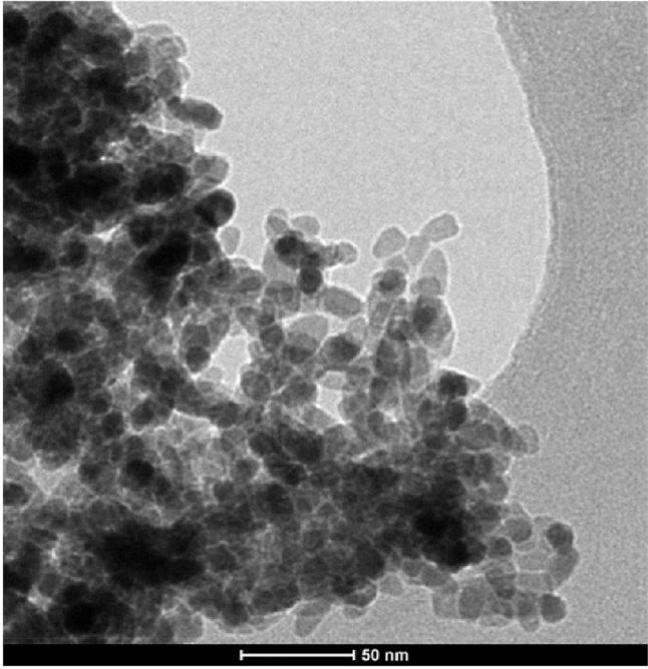


Fig. 3. TEM image of  $Zn_{0.9}Ga_{0.1}O$  nanocrystals.

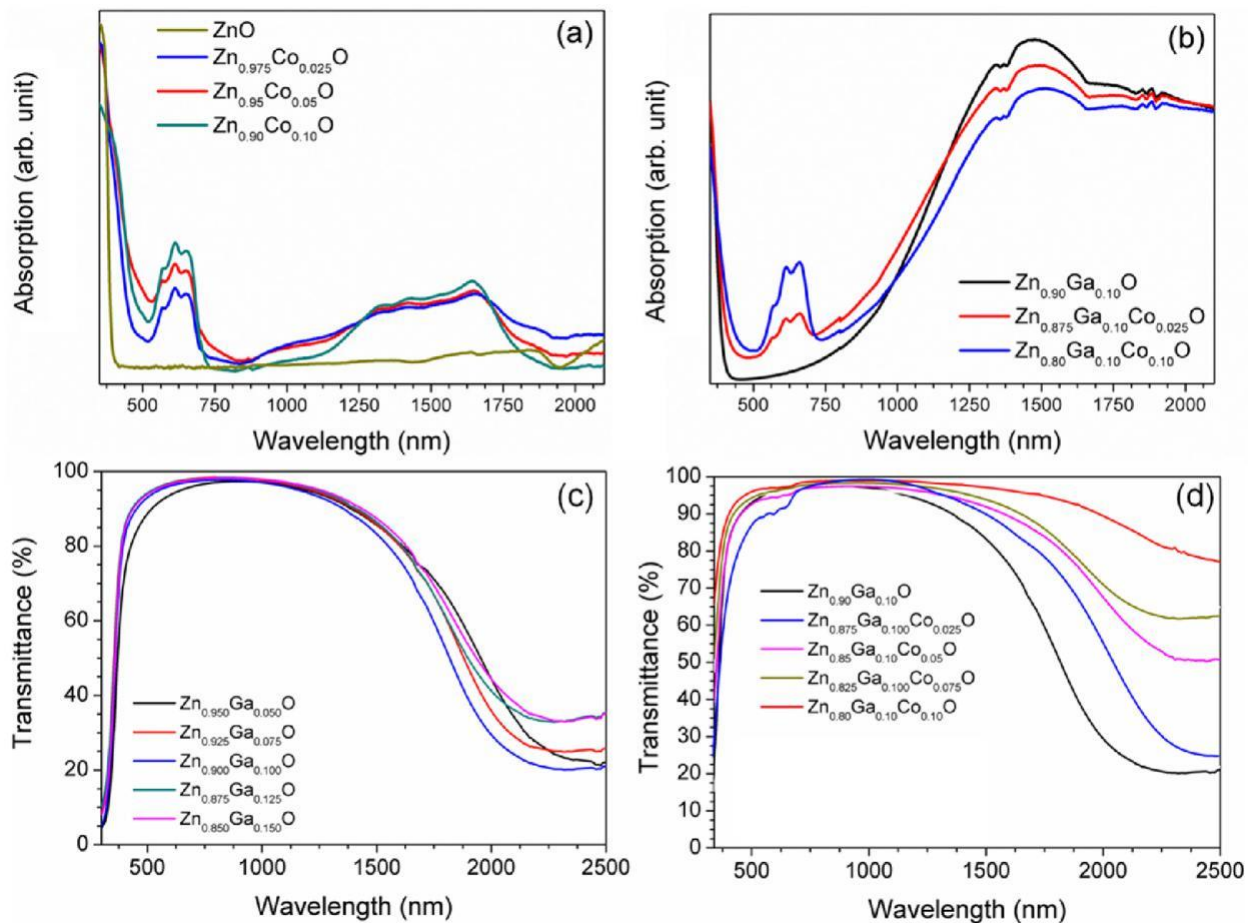
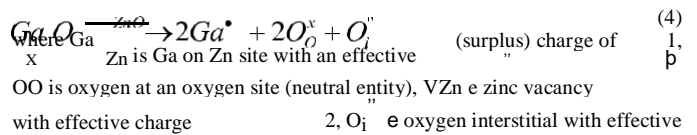
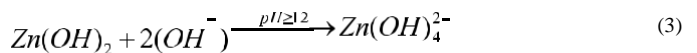


Fig. 4. Optical properties of sample powders and colloids. Kubelka-Munk UV-vis absorption spectra of Co-doped ZnO (a), as well as Ga-doped and Co-Ga co-doped ZnO (b) powders. Transmittance measurements for sample colloids are demonstrated in graphs (c) and (d).

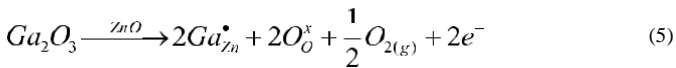
concentration indicates that the Co dopant prefers to substitute the  $Zn^{2\beta}$  (at its sites with tetrahedral oxygen coordination) even at higher Co content (viz.  $Zn_{0.9}Co_{0.1}O$ ).

Nanocrystals containing Ga exhibit a wide infrared absorption band attributed to plasmon resonance originating in aliovalent doping (Fig. 4 (b)). The observation of plasmon resonance in the GZO samples is an indication of the presence of delocalized (itinerant) charge carriers within the nanoparticles. The occurrence of a considerable delocalized charge carrier density (such that it would give rise to a plasmon resonance in the near IR) is not fully trivial even in the presence of an aliovalent dopant ( $Ga^{3\beta}$ ). Depending on synthesis conditions,  $Zn^{2\beta}$  substitution by  $Ga^{3\beta}$  can be expected to give rise to the formation of various point defects, the majority of which would be zinc vacancies,  $Ga^{3\beta}$  at  $Zn^{2\beta}$  sites, oxygen interstitials and/or free electrons. If GZO materials would be obtained under oxidizing conditions, the charge imbalance arising from  $Ga^{3\beta}$  at  $Zn^{2\beta}$  sites would become compensated either by zinc vacancies or oxygen interstitials in accordance to



charge 2.

On the other hand, under reducing conditions (viz. in ethanol solvothermal synthesis) the excess positive charge on Ga site is compensated by introducing electrons delocalized over the nano-particle according to the formula:



Upon Co co-doping of GZO, the optical density in the infrared region in Kubelka-Munk absorption spectra decreases, but, never-the-less, the Co-Ga co-doped ZnO nanocrystals still exhibit strong infrared (LSPR) adsorption, as well as clearly distinguishable ab-sorption bands from  $Co^{2p}$  at the tetrahedral  $Zn^{2p}$  lattice sites. The XRD results above and high kinetic energy photoelectron spec-troscopy (HAXPES) below reveal that some part of free electrons are consumed for reducing  $Co^{2p}$  to  $Co^0$  upon Co addition to GZO. Otherwise, the decrease of plasmonic absorbance intensity and energy, together with increase in saturation magnetization, has been taken as an indicator for electron mediated magnetic coupling in Mn-ITO and Fe-ITO systems [31].

The measured optical transmittance spectra of the nanocrystal colloids are demonstrated in Fig. 4 (c) and (d). GZO exhibit a broad absorption band in the near infrared range. The infrared absorption band is getting stronger with increasing Ga doping levels in ZnO until it attains the strongest near infrared absorption for the  $Zn_{0.9}Ga_{0.1}O$  sample, while the absorption gradually decreases with increasing co-dopant (cobalt) concentration. Samples with Ga concentrations above the  $Zn_{0.9}Ga_{0.1}O$  optimum show again some decrease in near infrared absorptivity, which may be because the substitutional dopant at higher concentrations can favor formation of self-compensating point defect clusters thus hindering forma-tion of any substantial free (delocalized) charge carrier density [50]. The formation of electronically neutral defect clusters at high

dopant concentration (sometimes called Frank and Kostlin $\epsilon$  clusters) is well reported in literature for transparent semiconductor oxides [51]. This is the main limitation for conductivity of transparent conductive oxides. However, even so, there is a huge number of itinerant charges at high hypervalent dopant level to contribute for magnetization.

Photoluminescence (PL) measurements were carried out to compare defect states in various samples. All samples demonstrate different PL spectral distribution under 266 nm laser excitation at 10K (Fig. 5 and supplementary Fig. S1) with the broader lumines-cence bands originating in ZnO intrinsic defects. The visible emis-sion in PL spectrum of undoped ZnO is related to the PL from electron and hole recombination in localized states with energy levels deep in the band gap originating from anion vacancies and/or interstitials in crystal lattice, whereas shallower defects are domi-nant in doped samples [52e54]. Exciton luminescence for undoped ZnO was 15 times higher than defect luminescence. For samples with Ga doping the exciton peak was not observed, which indicates higher point defect concentration in ZnO lattice.

By deconvoluting the complex luminescence bands of all sam-ples to Gaussian peaks, the typical ZnO intrinsic luminescence bands can be identified (Fig. 5). The luminescence band structure of ZnO is very complex [55], therefore multiple-peak fitting is disputable and challenging; however, such approach highlights the differences between the samples. All samples showed common intrinsic luminescence band peaking around 2.45eV (colored green in Fig. 5). This band is very typical for ZnO and originates from the recombination of photo-excited holes with singly-ionized oxygen vacancies [23,55,56] and the higher intensity of this band would indicate a larger oxygen vacancy concentration [56,57].

As demonstrated by equations (3) and (4) the  $Ga^{3p}$  doping may

trigger formation of oxygen interstitials and/or zinc vacancies. This correlates with luminescence observations where the blue band (~2.85eV) related to  $V_{Zn}$  is dominant for  $Ga^{3p}$  doped ZnO. PL measurements in combination with UV-vis absorption and trans-mittance measurements above show that there is mixture of point defects in  $Ga^{3p}$  doped ZnO samples, such as  $O_i$ ,  $V_{Zn}$  and itinerant electrons. This means there is ample room to increase plasmonic absorption in the infrared range for  $Ga^{3p}$  doped ZnO, which is important for infrared blocking smart window applications [58].

For Co doped samples an additional band at 3.15eV is visible. This band could be related to zinc interstitials [23,55]. In general, undoped ZnO sample shows more oxygen vacancy related lumi-nescence bands [55,59] and peaks of doped ZnO samples are con-nect with cation sublattice related defects.

Several samples were also studied using high kinetic energy photoelectron spectroscopy (HAXPES), which is a non-intrusive probe where the average probe depth can be varied by changing the excitation X-ray energy, as the inelastic mean free path (IMFP) of the photoelectrons in the sample (i.e., the depth at which the photoelectrons generated in the sample would be able to exit the sample, while still carrying the initial kinetic energy defined as the difference of the incident X-ray photon energy and the binding energy of the electron while in the sample in the ground state), which defines the mean probe depth, varies slowly with the photoelectron kinetic energy and approaches bulk sensitivity at high photoelectron kinetic energies. For the present purposes, the higher used incident X-ray photon energy of 6.9 keV with the IMFP above 8 nm at all edges (see detail below) can be considered a bulk probe, because the probe depth safely exceeds the radius of the nanoparticles of approximately 10 nm size (as seen using TEM in Fig. 3), whereas the XPS spectra at the lower excitation energy used (2.3 keV) will have some propensity for near-surface signal (IMFP-s on the order of 2e3 nm).

HAXPES spectral shapes of the metal 2p and oxygen 1s core levels were used mainly to study the bulk composition, but also to look for indications of any (radial) inhomogeneities of composition and/or charge states. Additional information regarding to use HAXPES is provided in Supplementary material.

In the Co 2p HAXPES (Fig. 6) we observe that although the Co is mainly oxidized (with the corresponding main  $Co^{2p}_{3/2}$  peak at slightly above 781 eV), there is a non-negligible presence of metallic Co in the bulk of the samples studied (see Fig. 6), which is spectrally relatively well distinguished at the leading edge of the Co 2p<sub>3/2</sub> level (the metallic Co peak is seen at approximately 778 eV binding energy, labelled  $Co^0$  in the figure). From the Co 2p<sub>3/2</sub> level relative peak intensities (i.e., the ratio of the Co 2p<sub>3/2</sub> spectral areas of the  $Co^0$  vs. the  $Co^{2p}$  components), we estimate the proportion of the reduced, metallic Co to amount to approximately 8e9% (as an upper limit) of the total contained cobalt for the more bulk sensi-tive XPS probe using the 6.9 keV incident X-ray energy, corre-sponding to a mean probe depth (IMFP) of ~85 Å for the Co 2p electrons) [60], while being considerably weaker when using the more shallow probe depth (2.3 keV incident X-rays, resulting in an estimated IMFP of ~26 Å for Co 2p), indicating that the reduced (metallic) Co preferentially appears at the core of the nanoparticles. It then becomes relevant to try to estimate the relative significance of the contribution of this metallic Co component to the overall magnetic response. On the background that magnetization values for TM NPs close to bulk magnetization values have been reported in the literature [61], the Co metal bulk magnetisation value of ~165 emu/g and the (metallic) Co percentage of the total mass, the contribution of the metallic Co to the overall magnetic response would have an upper limit at approximately 1.1 emu/g (for a 10% at. cationic Co content sample) or in the range of approximately 0.25e1.1 emu/g for the samples in this study (for more info see

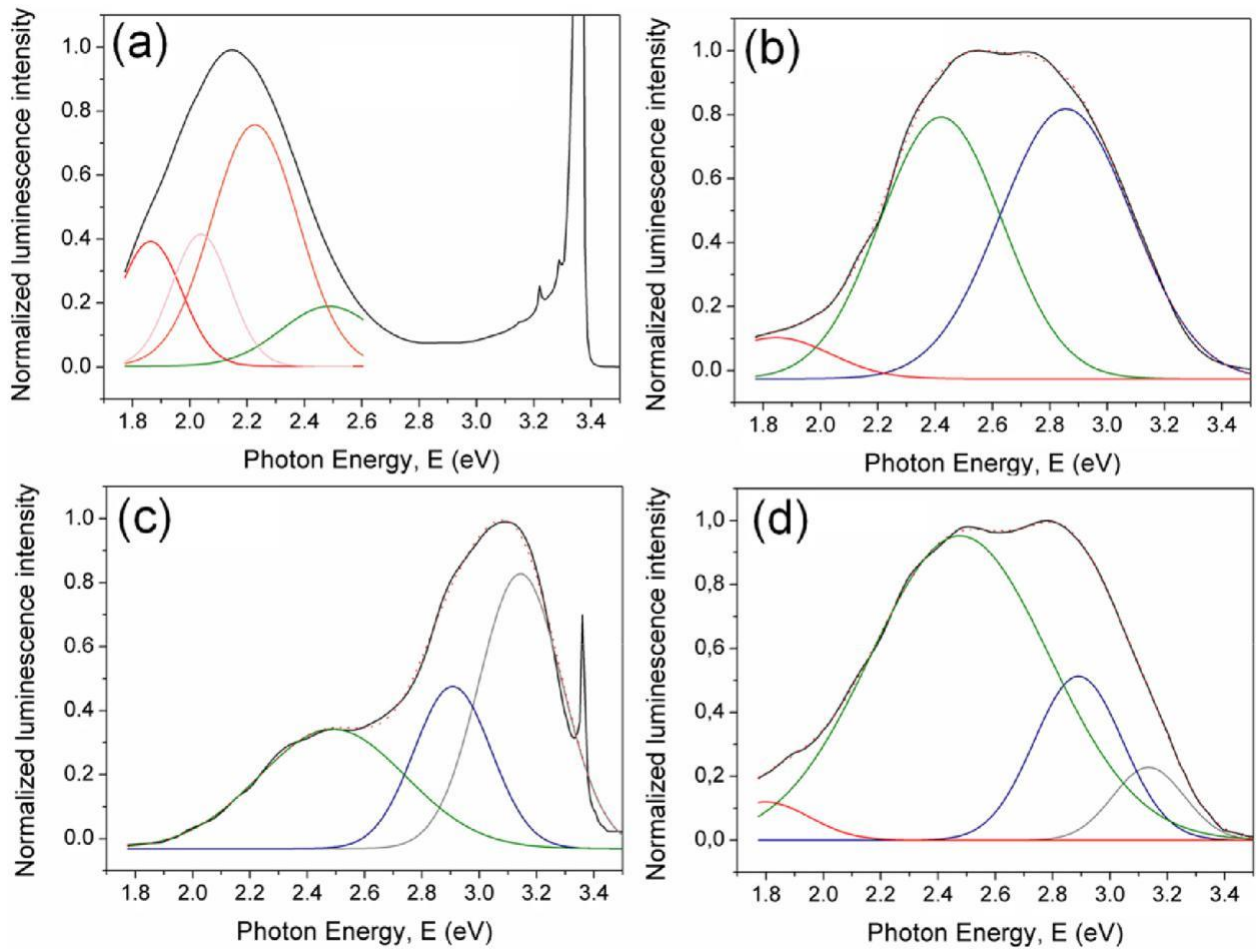


Fig. 5. Deconvoluted photoluminescence spectra for various nanocrystals: (a) ZnO, (b) Zn<sub>0.90</sub>Ga<sub>0.10</sub>O, (c) Zn<sub>0.95</sub>Co<sub>0.05</sub>O and (d) Zn<sub>0.90</sub>Ga<sub>0.05</sub>Co<sub>0.05</sub>O.

(Supplementary Material). While certainly not negligible, such contribution nevertheless still appears not to be defining the overall magnetic response with saturation values typically at several emu/g, as demonstrated below. However, an earlier XMCD (incl. element and orbital specific contributions to magnetic properties) report [62] on ZCO at different Co concentrations concluded from their data that the magnetic response is mainly due to (segregated) metallic Co clusters in their films (although Co was dominantly present as Co<sup>2+</sup> at T<sub>d</sub> ligand configuration, i.e. substituting at Zn sites). The antipodal differences in experimental observations can be related to differences in concentration of electronic point defects, although, need to consider also, that XMCD may not have yielded conclusive information due to limited probe depth.

The evolution of the O 1s XPS with introducing and increasing Ga content appears reminiscent of the observations of Yu et al. [63] with the change from a dominant single (lattice oxygen) peak in ZnO (and Co doped ZnO) to a spectrum with more weight at higher binding energy components, which correspond to lattice oxygen in the vicinity of a variety of introduced lattice defects.

In the O 1s spectra (Fig. 6), the major peak of ZnO lattice oxygen (below 531 eV binding energy) is seen to be accompanied by a smaller peak (marked by asterisk in the figure and typically attributed to hydroxyl groups at surface) at approximately 1.3 eV to higher binding energies also for the Co doped sample. The relative intensity of this latter peak is seen to depend on probe depth (being stronger for the less bulk sensitive probe) and indeed, as we have

earlier seen for un-doped and the Co doped ZnO nanoparticles with the conventional XPS applied in surface sensitive mode (with photoelectron kinetic energies in the range of 0.1 keV and the corresponding mean probe depth on the order of 5 Å), the surface hydroxyl related higher binding energy component has peak height comparable to that of lattice oxygen [42]. On this background it is telling that after introducing the aliovalent dopant (Ga), the relative intensities become insensitive to probe depth (as seen in Fig. 6), the varied incident X-ray energies give virtually identical spectra for the samples containing Ga), indicating that oxygen configuration becomes less unique throughout the nanoparticles (and not only at their surface).

Fig. 7 shows magnetization vs magnetic field strength curves at room temperature. Measured saturation magnetization values are presented in Supplementary Material, Table S1. All the measured Co doped ZnO samples (within the rather wide compositional range) exhibit ferromagnetic behavior. The un-doped ZnO nanocrystals do not exhibit ferromagnetic behavior. Magnetization curve of the pristine ZnO single crystalline nanowires at room temperature demonstrated in Supplementary Fig. S2 shows diamagnetic behavior, which is typical for bulk ZnO [64]. The M<sub>s</sub> grows gradually in both Zn<sub>0.9-x</sub>Co<sub>x</sub>Ga<sub>0.1</sub>O and Zn<sub>0.9-y</sub>Co<sub>0.05</sub>Ga<sub>y</sub>O systems with increasing Co or Ga concentration (x and y, respectively). Most interesting is gradual increase in magnetization with increasing Ga dopant, but, at the same time, keeping the Co content constant (at x = 0.05). A gradual increase in saturation magnetization from 1.48 to 3.96 emu/g is observed (2.7 fold increase) when Ga

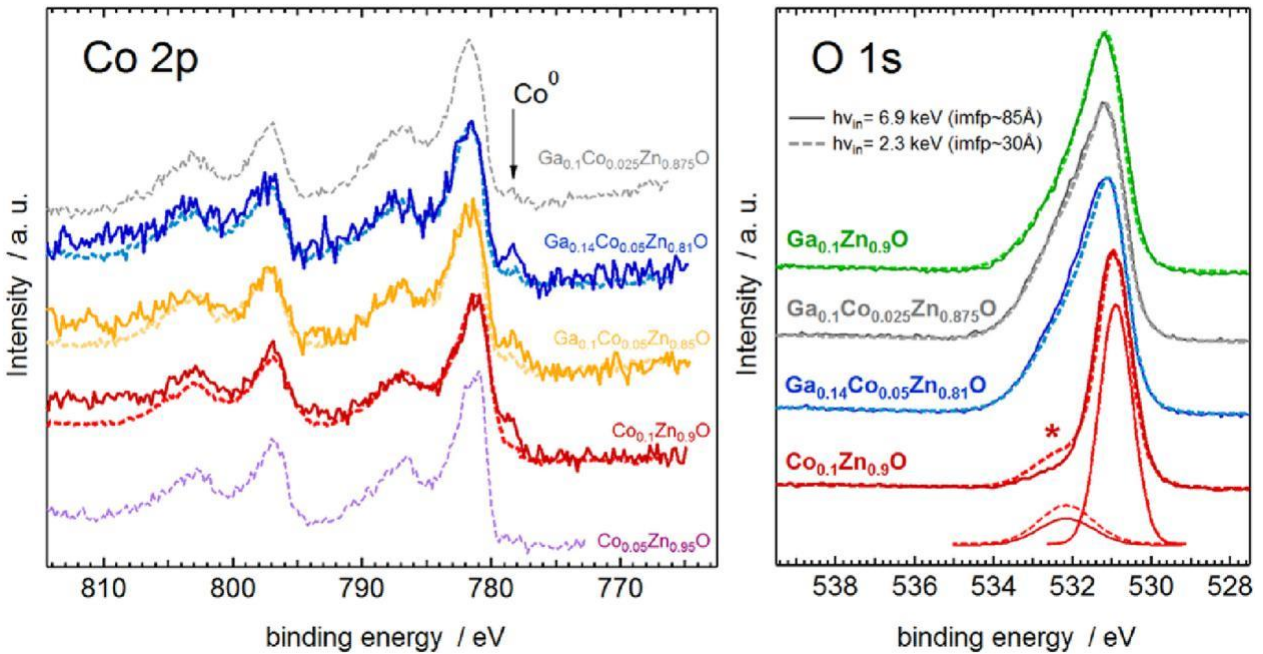


Fig. 6. Co 2p (left) and O 1s (right panel) XPS of select samples at two different incident X-ray energies: 2.3 keV and 6.9 keV, corresponding to mean probe depths  $\sim 30 \text{ \AA}$  (dashed lines) and  $\sim 85 \text{ \AA}$  (solid lines). Bottom (red) curves at the right panel: decomposition of the  $(\text{Co}_{0.1}\text{Zn}_{0.9}\text{O})$  O 1s spectra into the main peak at  $\sim 531 \text{ eV}$  corresponding to regular ( $\text{ZnO}$ ) crystal lattice sites, and the contribution at the high binding energy side (marked with an asterisk), which for Co doped samples appears surface (hydroxyl) related and it relatively decreases for the deeper probe (solid line), whereas for the Ga-Co codoped samples the deviating oxygen environments appear more evenly distributed throughout the nano-particles (show no dependence on probe depth). (For interpretation of the references to color in this figure legend, the reader is referred to the Web version of this article.)

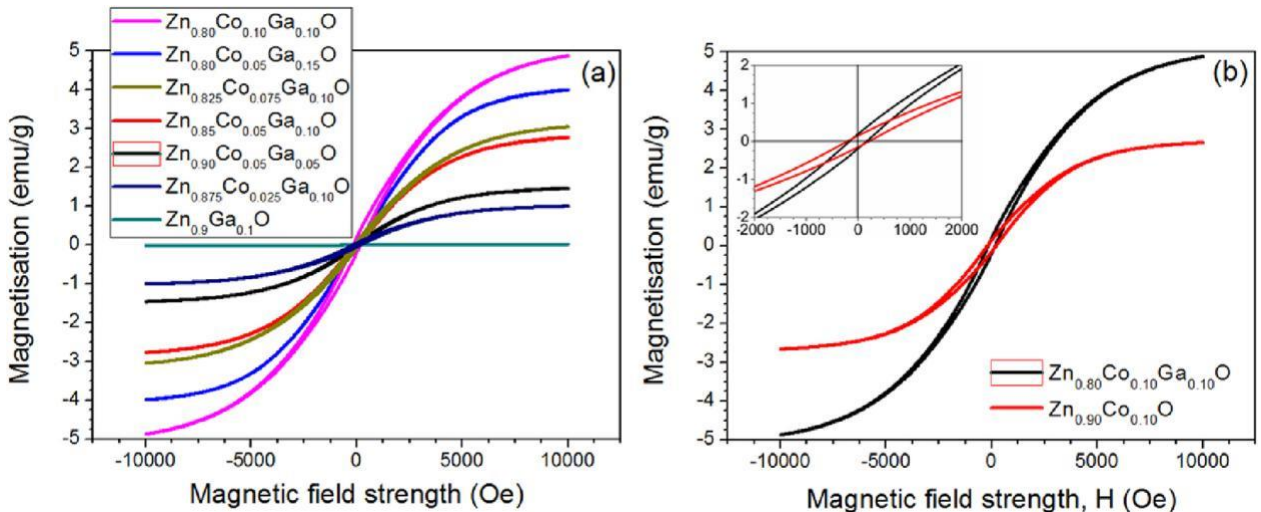


Fig. 7. Magnetization vs magnetic field strength curves at room temperature for various Co, Ga and Co-Ga co-doped  $\text{ZnO}$  nanocrystals. Inset on figure (b) close view of the hysteresis central part.

concentration is increased from 0.05 to 0.15 in composition  $\text{Zn}_{0.95-x}\text{Co}_{0.05}\text{Ga}_x\text{O}$ . The magnetization values clearly increase (double) from 2.65 emu/g to 4.88 emu/g also for highly doped  $\text{Zn}_{0.9}\text{Co}_{0.10}\text{O}$  and  $\text{Zn}_{0.8}\text{Co}_{0.10}\text{Ga}_{0.10}\text{O}$  nanocrystals. To the best of our knowledge we observed room temperature saturation magnetization higher than previously reported values for multifunctional magnetic and plasmonic nanocrystals as depicted in Table 1. The observed saturation magnetization values are also 2 orders of magnitude higher than Ga doped  $\text{ZnO}$ , which exhibit room temperature ferromagnetic behavior with saturation magnetization 0.011 emu/g, as demonstrated in supplementary Fig. S3. A paramagnetic contribution to the overall shape of the magnetic response curves should

Table 1  
Room temperature saturation magnetization ( $M_s$ ) values for different magnetic plasmonic nanocrystals reported in literature.

Material	$M_s$ (emu/g)	Reference
Mn Sn codoped $\text{In}_2\text{O}_3$	2.52	[31]
$\text{Sn}^{4p}$ -doped $(\text{InFe}_{0.04})_2\text{O}_3$	0.37	[33]
Sn- and Fe-codoped $\text{In}_2\text{O}_3$	0.05	[35]
Co- and Ga-codoped $\text{ZnO}$	4.88	This work

certainly be considered and we find the shapes of the curves (which we observe to level out at higher external fields) not to support a

dominant paramagnetic component in the overall signal.

The observed increase in saturation magnetization ( $M_s$ ) when introducing the  $\text{Ga}^{3\beta}$  suggests that the extra loosely bound delocalized electrons now available in the lattice should be relevant in activating new ferromagnetic interactions even if clustering of the magnetic ions cannot be fully ruled out [31]. Park et al. have stated that nanometer-sized segregated TM clusters are responsible for the room temperature ferromagnetic behavior in the (otherwise paramagnetic) Co doped ZnO and that clustering occurs for compositions with Co loading  $x > 0.12$  in  $\text{Zn}_{1-x}\text{Co}_x\text{O}$  [65]. However, our (HAXPES) estimates (above) show that the relative amount of reduced Co (as it can be expected to be segregated in metallic clusters) can produce a non-negligible contribution to the overall magnetic response, whereas the overall measured response of the nanoparticles still remains several (4e5) times stronger than only magnetizing the segregated clusters would allow. We therefore find that the observed increase in saturation magnetization ( $M_s$ ) when introducing the hypervalent  $\text{Ga}^{3\beta}$  dopant suggests that the resulting extra delocalized electron density in the nanoparticles not only gives rise to plasmonic properties (e.g. as exposed in the LSPR absorption) but also, according to a mechanism previously reported for different materials [31], promotes itinerant electron mediated (Stoner) magnetism.

## 4. Conclusions

We establish Ga and Co co-doping of ZnO to obtain diluted magnetic degenerated semiconductor oxide nanocrystals. Our results confirm that a considerable delocalized electron density is established, which contributes significantly to the magnetic exchange coupling. Ga doping primarily introduces strong plasmonic absorption in the infrared range, while Co doping gives rise to ferromagnetic properties to the ZnO nanocrystals. Further, we observe an increase in the saturation magnetization ( $M_s$ ) when introducing the hypervalent  $\text{Ga}^{3\beta}$ , which suggests that the introduced delocalized electron density becomes relevant in promoting itinerant electron mediated exchange interactions.

## Acknowledgements

Authors kindly acknowledge to the Estonian Research Council (PUT1096, IUT2-25, PUT735), the Estonian Centre of Excellence in Research project "Advanced materials and high-technology devices for sustainable energetics, sensorics and nanoelectronics (TK141), and the financial support of HZB. We are grateful to the staff of BESSY II for the assistance and co-operation during the synchrotron-based measurements.

## References

- [1] R. Buonsanti, A. Llordes, S. Aloni, B.A. Helms, D.J. Milliron, Tunable infrared absorption and visible transparency of colloidal aluminum-doped zinc oxide nanocrystals, *Nano Lett.* 11 (2011) 4706e4710.
- [2] A.M. Schimpf, S.T. Ochsenbeina, R. Buonsanti, D.J. Milliron, D.R. Gamelin, Comparison of extra electrons in colloidal n-type  $\text{Al}^{3\beta}$ -doped and photo-chemically reduced ZnO nanocrystals, *Chem. Commun.* 48 (2012) 9352e9354.
- [3] E.D. Gaspera, A.S.R. Chesman, J. van Embden, J.J. Jasieniak, Non-injection synthesis of doped zinc oxide plasmonic nanocrystals, *ACS Nano* 8 (2014) 9154e9163.
- [4] J. Kim, G.V. Naik, A.V. Gavrilenko, K. Dondapati, V.I. Gavrilenko, S.M. Prokes, O.J. Glembocki, V.M. Shalaev, A. Boltasseva, Optical properties of gallium-doped zinc oxided low-loss plasmonic material: first-principles theory and experiment, *Phys. Rev. X* 3 (2013), 041037.
- [5] M. Saha, S. Ghosh, V.D. Ashok, S.K. De, Carrier concentration dependent optical and electrical properties of Ga doped ZnO hexagonal nanocrystals, *Phys. Chem. Chem. Phys.* 17 (2015) 16067e16079.
- [6] E.D. Gaspera, N.W. Duffy, J. van Embden, L. Waddington, L. Bourgeois, J.J. Jasieniak, A.S.R. Chesman, Plasmonic Ge-doped ZnO nanocrystals, *Chem. Commun.* 51 (2015) 12369e12372.
- [7] X. Liang, Y. Ren, S. Bai, N. Zhang, X. Dai, X. Wang, H. He, C. Jin, Z. Ye, Q. Chen, L. Chen, J. Wang, Y. Jin, Colloidal indium-doped zinc oxide nanocrystals with tunable work function: rational synthesis and optoelectronic applications, *Chem. Mater.* 26 (2014) 5169e5178.
- [8] S.D. Lounis, E.L. Runnerstrom, A. Bergerud, D. Nordlund, D.J. Milliron, Defect chemistry and plasmon physics of colloidal metal oxide nanocrystals, *J. Am. Chem. Soc.* 136 (2014) 7110e7116.
- [9] Y. Li, W. Lu, Q. Huang, C. Li, W. Chen, Copper sulfide nanoparticles for photo-thermal ablation of tumor cells, *Nanomedicine* 5 (2010) 1161e1171.
- [10] A. Llordes, Y. Wang, A. Fernandez-Martinez, P. Xiao, T. Lee, A. Poulin, O. Zandi, C.A.S. Cabezas, G. Henkelman, D.J. Milliron, Linear topology in amorphous metal oxide electrochromic networks obtained via low-temperature solution processing, *Nat. Mater.* 15 (2016) 1267e1273.
- [11] T.E. Williams, C.M. Chang, E.L. Rosen, G. Garcia, E.L. Runnerstrom, B.L. Williams, B. Koo, R. Buonsanti, D.J. Milliron, B.A. Helms, NIR-selective electrochromic heteromaterial frameworks: a platform to understand meso-scale transport phenomena in solid-state electrochemical devices, *J. Mater. Chem. C* 2 (2014) 3328e3335.
- [12] G. Garcia, R. Buonsanti, A. Llordes, E.L. Runnerstrom, A. Bergerud, D.J. Milliron, Near-infrared spectrally selective plasmonic electrochromic thin films, *Adv. Opt. Mater.* 1 (2013) 215e220.
- [13] E.L. Runnerstrom, A. Llordes, S.D. Lounisa, D.J. Milliron, Nanostructured electrochromic smart windows: traditional materials and NIR-selective plasmonic nanocrystals, *Chem. Commun.* 50 (2014) 10555e10572.
- [14] A. Sutka, M. Timusk, N. Dobelin, R. Parna, M. Visnapuu, U. Joost, T. Kaambre, V. Kisand, K. Saal, M. Knite, A straightforward and "green" solvothermal synthesis of Al doped zinc oxide plasmonic nanocrystals and piezoresistive elastomer nanocomposite, *RSC Adv.* 5 (2015) 63846e63852.
- [15] L.D. Trizio, R. Buonsanti, A.M. Schimpf, A. Llordes, D.R. Gamelin, R. Simonutti, D.J. Milliron, Nb-doped colloidal  $\text{TiO}_2$  nanocrystals with tunable infrared absorption, *Chem. Mater.* 25 (2013) 3383e3390.
- [16] B.T. Diroll, T.R. Gordon, E.A. Gaulding, D.R. Klein, T. Paik, H.J. Yun, E.D. Goodwin, D. Damodhar, C.R. Kagan, C.B. Murray, Synthesis of N-type plasmonic oxide nanocrystals and the optical and electrical characterization of their transparent conducting films, *Chem. Mater.* 26 (2014) 4579e4588.
- [17] S.S.K. Guduru, I. Kriegel, R. Ramponi, F. Scotognella, Plasmonic heavily-doped semiconductor nanocrystal dielectrics: making static photonic crystals dynamic, *J. Phys. Chem. C* 119 (2015) 2775e2782.
- [18] J.N. Anker, W.P. Hall, O. Lyandres, N.C. Shah, J. Zhao, R.P. van Duyne, Bio-sensing with plasmonic nanosensors, *Nat. Mater.* 7 (2008) 442e453.
- [19] X. Ye, J. Fei, B.T. Diroll, T. Paik, C.B. Murray, Expanding the spectral tunability of plasmonic resonances in doped metal-oxide nanocrystals through cooperative cation/eanion codoping, *J. Am. Chem. Soc.* 136 (2014) 11680e11686.
- [20] G. Clavel, M.-G. Willinger, D. Zitoun, N. Pinna, Solvent dependent shape and magnetic properties of doped ZnO nanostructures, *Adv. Funct. Mater.* 17 (2007) 3159e3169.
- [21] M. Bouloudenine, N. Viart, S. Colis, J. Kortus, A. Dinia, Antiferromagnetism in bulk  $\text{Zn}_1-x\text{Co}_x\text{O}$  magnetic semiconductors prepared by the coprecipitation technique, *Appl. Phys. Lett.* 87 (2005) 052501.
- [22] S.W. Yoon, S.-B. Cho, S.C. We, S. Yoon, B.J. Suh, Magnetic properties of ZnO-based diluted magnetic semiconductors, *J. Appl. Phys.* 93 (2003) 7879e7881.
- [23] G.H. Mhlongo, K. Shingange, Z.P. Tshabalala, B.P. Dhonge, F.A. Mahmoud, B.W. Mwakikunga, D.E. Motaung, Room temperature ferromagnetism and gas sensing in ZnO nanostructures: influence of intrinsic defects and Mn, Co, Cu doping, *Appl. Surf. Sci.* 390 (2016) 804e815.
- [24] H.W. Zhang, Z.R. Wei, Z.Q. Li, G.Y. Dong, Room-temperature ferromagnetism in Fe-doped, Fe- and Cu-codoped ZnO diluted magnetic semiconductor, *Mater. Lett.* 61 (2007) 3605e3607.
- [25] D.A. Schwartz, K.R. Kittilstved, D.R. Gamelin, Above-room-temperature ferromagnetic  $\text{Ni}^{2\beta}$ -doped ZnO thin films prepared from colloidal diluted magnetic semiconductor quantum dots, *Appl. Phys. Lett.* 85 (2004) 1395e1397.
- [26] L.T. Chang, C.Y. Wang, J. Tang, T. Nie, W. Jiang, C.P. Chu, S. Arifin, L. He, M. Afsal, L.J. Chen, K.L. Wang, Electric-field control of ferromagnetism in Mn-doped ZnO nanowires, *Nano Lett.* 14 (2014) 1823e1829.
- [27] P. Sharma, A. Gupta, K.V. Rao, F.J. Owens, R. Sharma, R. Ahuja, J.M.O. Guillen, B. Johansson, G.A. Gehring, Ferromagnetism above room temperature in bulk and transparent thin films of Mn-doped ZnO, *Nat. Mater.* 2 (2003) 673e677.
- [28] D.E. Motaung, I. Kortidis, G.H. Mhlongo, M.-M. Duvenhage, H.C. Swart, G. Kiriacidis, S.S. Ray, Correlating the magnetism and gas sensing properties of Mn-doped ZnO films enhanced by UV irradiation, *RSC Adv.* 6 (2016) 26227e26238.
- [29] D.A. Schwartz, D.R. Gamelin, Reversible 300 K ferromagnetic ordering in a diluted magnetic semiconductor, *Adv. Mater.* 16 (2004) 2115e2119.
- [30] S.T. Ochsenbein, Y. Feng, K.M. Whitaker, E. Badaeva, W.K. Liu, X. Li, D.R. Gamelin, Charge-controlled magnetism in colloidal doped semiconductor nanocrystals, *Nat. Nanotechnol.* 4 (2009) 681e687.
- [31] B. Tandon, A. Yadav, A. Nag, Delocalized electrons mediated magnetic coupling in Mn Sn codoped  $\text{In}_2\text{O}_3$  nanocrystals: plasmonics shows the way,

- Chem. Mater. 28 (2016) 3620e3624.
- [32] A. Yadav, B. Tandon, A. Nag, Reduction of Mn<sup>3p</sup> to Mn<sup>2p</sup> and near infrared plasmonics from Mn<sub>x</sub>Sn codoped In<sub>2</sub>O<sub>3</sub> nanocrystals, RSC Adv. 6 (2016) 79153e79159.
- [33] S. Qaseem, M. Naeem, S.R. Ali, M. Maqbool, S.I. Ali, Tunable High-T<sub>C</sub> ferromagnetism in Sn<sup>4p</sup>-doped (InFe<sub>0.04</sub>)<sub>2</sub>O<sub>3</sub> nanoparticles: a vital role of electron doping, Mater. Technol. 32 (2016) 3276e333.
- [34] G.S. Shanker, B. Tandon, T. Shibata, S. Chattopadhyay, A. Nag, Doping controls plasmonics, electrical conductivity, and Carrier-mediated magnetic coupling in Fe and Sn codoped In<sub>2</sub>O<sub>3</sub> nanocrystals: local structure is the key, Chem. Mater. 27 (2015) 892e900.
- [35] B. Tandon, G.S. Shanker, A. Nag, Multifunctional Sn- and Fe-codoped In<sub>2</sub>O<sub>3</sub> colloidal nanocrystals: plasmonics and magnetism, J. Phys. Chem. Lett. 5 (2014) 2306e2311.
- [36] N.S. Garnet, V. Ghodsi, L.N. Hutzliss, P. Yin, M. Hegde, P.V. Radovanovic, Probing the role of dopant oxidation state in the magnetism of diluted magnetic oxides using Fe-doped In<sub>2</sub>O<sub>3</sub> and SnO<sub>2</sub> nanocrystals, J. Phys. Chem. C 121 (2017) 1918e1927.
- [37] I. Bilecka, I. Djerdj, M. Niederberger, One-minute synthesis of crystalline bi-nary and ternary metal oxide nanoparticles, Chem. Commun. 7 (2008) 886e888.
- [38] T. Kotsukechagia, F. Cellesi, A. Thomas, M. Niederberger, N. Tirelli, Preparation of ligand-free TiO<sub>2</sub> (anatase) nanoparticles through a nonaqueous process and their surface functionalization, Langmuir 24 (2008) 6988e6997.
- [39] K. Rode, A. Anane, R. Mattana, J.-P. Contour, O. Durand, R. Le Bourgeois, Magnetic semiconductors based on cobalt substituted ZnO, J. Appl. Phys. 93 (2003) 7676e7678.
- [40] J.H. Park, M.G. Kim, H.M. Jang, S. Ryu, Y.M. Kim, Co-metal clustering as the origin of ferromagnetism in Co-doped ZnO thin films, Appl. Phys. Lett. 84 (2004) 1338e1340.
- [41] J.M.D. Coey, M. Venkatesan, C.B. Fitzgerald, Donor impurity band exchange in dilute ferromagnetic oxides, Nat. Mater. 4 (2005) 173e179.
- [42] A. Sutka, T. Kaambre, R. Parna, I. Juhnevica, M. Maiorov, U. Joost, V. Kisand, Co-doped ZnO nanowires as visible light photocatalysts, Solid State Sci. 56 (2016) 54e62.
- [43] A. Sutka, M. Timusk, A. Loot, U. Joost, T. Kaambre, Polarizable nanowire colloids for power free naked eye optical detection of electrostatic surface charges, Adv. Mater. Technol. 1 (2016), 1600154.
- [44] F. Schafers, The crystal monochromator beamline KMC-1 at BESSY II, JLSRF 2 (2016) A96.
- [45] K. Ueda, H. Tabata, T. Kawai, Magnetic and electric properties of transition-metal-doped ZnO films, Appl. Phys. Lett. 79 (2001) 988e990.
- [46] B. Cheng, E.T. Samulski, Hydrothermal synthesis of one-dimensional ZnO nanostructures with different aspect ratios, Chem. Commun. 10 (2004) 980e987.
- [47] R. Chen, P. Zhu, L. Deng, T. Zhao, R. Sun, C. Wong, Effect of aluminum doping on the growth and optical and electrical properties of ZnO nanorods, Chem.-PlusChem 79 (2014) 743e750.
- [48] L. Grigorjeva, D. Millers, K. Smits, J. Grabis, J. Fidelus, W. Łojkowski, T. Chudoba, K. Bienkowski, The luminescence of ZnO ceramics, Radiat. Meas. 45 (2010) 441e443.
- [49] P. Koidl, Optical absorption of Co<sup>2p</sup> in ZnO, Phys. Rev. B 15 (1977) 2493e2499.
- [50] G. Frank, H. Kostlin, Electrical properties and defect model of tin-doped indium oxide layers, Appl. Phys. A 27 (1982) 197e206.
- [51] O. Warschkow, D.E. Ellis, G.B. Gonzalez, T.O. Mason, Defect cluster aggregation and nonreducibility in tin-doped indium oxide, J. Am. Ceram. Soc. 86 (2003) 1707e1711.
- [52] H. Fu, T. Xu, S. Zhu, Y. Zhu, Photocorrosion inhibition and enhancement of photocatalytic activity for ZnO via hybridization with C60, Environ. Sci. Technol. 42 (2008) 8064e8069.
- [53] D.S. Bohle, C.J. Spina, Cationic and anionic surface binding sites on nano-crystalline zinc oxide: surface influence on photoluminescence and photo-catalysis, J. Am. Chem. Soc. 131 (2009) 4397e4404.
- [54] J.W. Soares, J.E. Whitten, D.W. Oblas, D.M. Steeves, Novel photoluminescence properties of surface-modified nanocrystalline zinc oxide: toward a reactive scaffold, Langmuir 24 (2008) 371e374.
- [55] Ü. Ozgür, Y.I. Alivov, C. Liu, A. Teke, M.A. Reshchikov, S. Dogan, V. Avrutin, S.-J. Cho, H. Morkoç, A comprehensive review of ZnO materials and devices, J. Appl. Phys. 98 (2005), 041301.
- [56] B. Lin, Z. Fu, Y. Jia, Green luminescent center in undoped zinc oxide films deposited on silicon substrates, Appl. Phys. Lett. 79 (2001) 943e945.
- [57] L. Grigorjeva, D. Millers, K. Smits, A. Zolotarjovs, Gas sensitive luminescence of ZnO coatings obtained by plasma electrolytic oxidation, Sensor. Actuator. A 234 (2015) 290e293.
- [58] R. Buonsanti, A. Llordes, S. Aloni, B.A. Helms, D.J. Milliron, Tunable infrared absorption and visible transparency of colloidal aluminum-doped zinc oxide nanocrystals, Nano Lett. 11 (2011) 4706e4710.
- [59] D.E. Motaung, G.H. Mhlongo, S.S. Nkosi, G.F. Malgas, B.W. Mwakikunga, E. Coetsee, H.C. Swart, H.M.I. Abdallah, T. Moyo, S.S. Ray, Shape-selective dependence of room temperature ferromagnetism induced by hierarchical ZnO nanostructures, ACS Appl. Mater. Interfaces 6 (2014) 8981e8995.
- [60] S. Tanuma, C.J. Powell, D.R. Penn, Calculations of electron inelastic mean free paths. V. Data for 14 organic compounds over the 50e2000 eV range, Surf. Interface Anal. 21 (1994) 165e176.
- [61] L.M. Parkes, R. Hodgson, L.T. Lu, L.D. Tung, I. Robinson, D.G. Fernig, N.T.K. Thanh, Cobalt nanoparticles as a novel magnetic resonance contrast agent - relaxivities at 1.5 and 3 Tesla, Contrast Media Mol. Imaging 3 (2008) 150e156.
- [62] K. Rode, R. Mattana, A. Anane, V. Cros, E. Jacquet, J.-P. Contour, F. Petroff, A. Fert, M.-A. Arrio, Ph. Sainctavit, P. Bencok, F. Wilhelm, N.B. Brookes, A. Rogalev, Magnetism of (Zn,Co)O thin films probed by x-ray absorption spectroscopies, Appl. Phys. Lett. 92 (2008), 012509.
- [63] C.F. Yu, S.H. Chen, S.J. Sun, H. Chou, Influence of the grain boundary barrier height on the electrical properties of Gallium doped ZnO thin films, Appl. Surf. Sci. 257 (2011) 6498e6502.
- [64] M. Kapilashrami, J. Xu, V. Strom, K.V. Rao, L. Belova, Transition from ferromagnetism to diamagnetism in undoped ZnO thin films, Appl. Phys. Lett. 95 (2009), 033104.
- [65] J.H. Park, M.G. Kim, H.M. Jang, S. Ryu, Y.M. Kim, Co-metal clustering as the origin of ferromagnetism in Co-doped ZnO thin films, Appl. Phys. Lett. 84 (2004) 1338e1340.